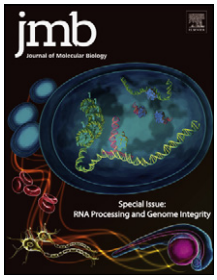

Comprehensive Identification of Nuclear and Cytoplasmic TNRC6A-Associating Proteins

Masataka Suzawa[1], Kentaro Noguchi[2], Kenji Nishi[1], Hiroko Kozuka-Hata[3], Masaaki Oyama[3] and Kumiko Ui-Tei[1,2]

1 - Department of Biological Sciences, *Graduate School of Science, The University of Tokyo, Tokyo 113-0033, Japan*
2 - Department of Computational Biology and Medical Sciences, *Graduate School of Frontier Sciences, The University of Tokyo, Chiba-ken 277-8651, Japan*
3 - Medical Proteomics Laboratory, *The Institute of Medical Science, The University of Tokyo, Tokyo 108-8639, Japan*

Correspondence to Kumiko Ui-Tei: *Department of Biological Sciences, Graduate School of Science, The University of Tokyo, Tokyo 113-0033, Japan. ktei@bs.s.u-tokyo.ac.jp*
http://dx.doi.org/10.1016/j.jmb.2017.04.017

Abstract

Trinucleotide repeat-containing gene 6A protein (TNRC6A) is an essential protein for microRNA-mediated gene silencing. TNRC6A functions in the cytoplasm as a platform protein interacting with Argonaute protein, on which microRNA is loaded for RNA silencing, and decapping enzymes or deadenylation protein complexes to induce mRNA degradation. We previously revealed that TNRC6A shuttles between the cytoplasm and nucleus. However, the function of TNRC6A in the nucleus is unclear. Here, we performed a comprehensive identification of the nuclear and cytoplasmic interacting proteins of TNRC6A protein by mass spectrometry and identified multiple proteins involved in the nuclear and cytoplasmic complexes. We found that many RNA degradation pathway proteins were involved in both nuclear and cytoplasmic TNRC6A complexes, suggesting that RNA silencing may occur via TNRC6A in both nucleus and cytoplasm or that they were involved in other important function in the nucleus. Furthermore, proteins identified in the nuclear TNRC6A complex were categorized into the spliceosomal pathway. This may mean that TNRC6A regulates splicing in the nucleus. In contrast, pathogen infection- and RNA transport-associated proteins were identified in the cytoplasmic TNRC6A complex. Thus, TNRC6A may be also involved in these pathways in the cytoplasm.

Introduction

Trinucleotide repeat-containing gene 6A protein (TNRC6A) was first identified as an autoantigen from sera of patient suffering from motor and sensory neuropathies [1]. It was designated as GW182, since it is a 182-KDa protein containing multiple glycine-tryptophan repeats, one or more glutamine-rich (Q-rich) region, and a classical RNA recognition motif (RRM) at the C terminus. GW182 belongs to an evolutionarily conserved protein family restricted to metazoans, which includes AIN-1 and AIN-2 from *Caenorhabditis elegans* [2,3] and Gawky from *Drosophila melanogaster* [4]. Vertebrates have three paralogs, GW182/TNRC6A, TNRC6B, and TNRC6C, which are located in the cytoplasmic processing body [5]. All three members associate with Argonaute (AGO) family members, AGO1–4, through their N-terminal GW-motifs in the microRNA (miRNA)-induced silencing complex [6]. TNRC6A/B/C then promotes translational repression and/or degradation of miRNA targets mediated by their C-terminal silencing domains. Extensive *in vitro* studies showed that the interaction of GW182 with other components of the processing body, such as PAN2-PAN3 and carbon catabolite repression 4 (CCR4)-CCR4-associated factor 1 (CAF1) deadenylase complexes, promotes mRNA deadenylation [7].

Recently, we revealed that human TNRC6A has a nuclear localization signal (NLS) and a nuclear export signal (NES) and shuttles between the nucleus and cytoplasm [8]. In several human

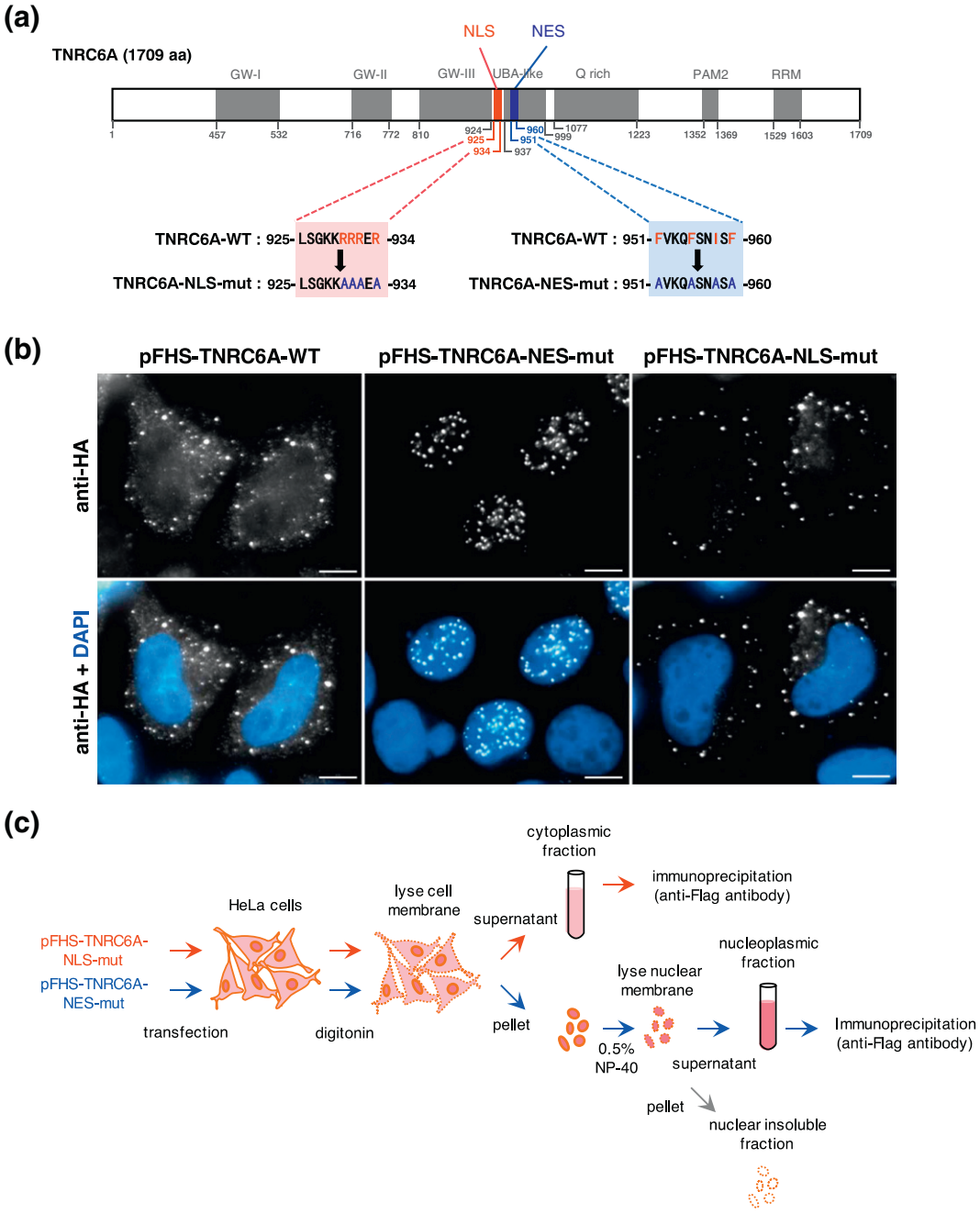

Fig. 1. Domain structure and subcellular localization of human TNRC6A protein and cell fractionation procedure. (a) Domain structure of TNRC6A protein. Gray boxes indicate GW repeats (GW-I, GW-II, GW-III domains), UBA-like domain, a Q-rich region, a poly(A)-binding protein binding motif 2 (PAM2), and an RRM. Numbers denote the amino acid position relative to the N terminus. Red box indicates NLS, and sequences of NLS and NLS-mut were shown below the domain structure. Blue box indicates NES, and sequences of NES and NES-mut were shown below the domain structure. (b) Subcellular localization of TNRC6A-WT, TNRC6A-NES-mut, and TNRC6A-NLS-mut proteins in the cells transfected with each expression plasmid. Upper panels show the cells stained with Cy3-conjugated anti-HA antibody. Lower panels show the merged images with DAPI (blue). Bar represents 10 μm. (c) Procedure for cell fractionation. pFHS-TNRC6A-NLS-mut or pFHS-TNRC6A-NES-mut was transfected into HeLa cells, and the cells were lysed with digitonin and centrifuged. The supernatant was used as the cytoplasmic fraction. The pellet was further lysed with NP-40, and the supernatant following centrifugation was used as the nuclear fraction. Both fractions were immunoprecipitated with anti-Flag antibody.

cancers, such as gastric, colorectal, prostate, and esophageal, TNRC6A protein is mainly localized in the nucleus [9,10]. Thus, the major subcellular localization of TNRC6A is not the same in all cell types, although the functional purpose of subcellular localization remains unknown.

To unlock the nuclear function of TNRC6A, we comprehensively identified proteins interacting with nuclear and cytoplasmic TNRC6A by immunoprecipitation (IP) and mass spectrometry (MS) analyses. Both nuclear and cytoplasmic TNRC6A commonly interact with multiple proteins associated with RNA degradation. In addition, we also revealed that nuclear and cytoplasmic TNRC6A interact with different sets of proteins associated with splicing, pathogen infection, and RNA transport pathways.

Results

Isolation of nuclear and cytoplasmic TNRC6A protein complexes

Human TNRC6A protein shares a common structural organization with vertebrate and insect homologs due to five characteristic regions: multiple glycine-tryptophan repeats, a central ubiquitin-associated (UBA)-like domain, a Q-rich region, a poly(A)-binding protein binding motif 2, and a C-terminal RRM (Fig. 1a). In our previous report [8], we revealed that human TNRC6A shuttles between the nucleus and cytoplasm via the NLS and NES in the central region. When a wild-type Flag-, HA-, and streptavidin-binding peptide (FHS)-tagged TNRC6A expression construct (pFHS-TNRC6A-WT) was transfected into human HeLa cells and detected with anti-HA antibody, TNRC6A-WT was mainly observed in the cytoplasm compared to control cells stained with 4′-6-diamidino-2-phenylindole (DAPI; Fig. 1b). However, TNRC6A with a NES mutation (TNRC6A-NES-mut) was mainly localized to the nucleus (Fig. 1b), and TNRC6A with an NLS mutation (TNRC6A-NLS-mut) was predominantly localized to the cytoplasm, similar to TNRC6A-WT. Thus, TNRC6A is distributed in the cytoplasm in HeLa cells but usually shuttles between the nucleus and the cytoplasm. It has been confirmed that the subcellular localizations of overexpressed TNRC6A proteins with NLS or NES mutation were essentially consistent with those expressed at the endogenous levels in our previous report [8].

To identify proteins interacting with nuclear and cytoplasmic TNRC6A, we used TNRC6A-NES-mut or TNRC6A-NLS-mut protein in IP. Nuclear and cytoplasmic fractions were separated from HeLa cells transfected with either pFHS-TNRC6A-NES-mut or pFHS-TNRC6A-NLS-mut plasmid (Fig. 1c). Cell membranes from cells transfected with pFSH-TNRC6A-NES-mut or pFSH-TNRC6A-NLS-mut were dissolved with digitonin, and the centrifuged supernatant was designated as the cytoplasmic fraction. The precipitate from cells transfected with pFSH-TNRC6A-NES-mut was further lysed with 0.5% NP-40, and the centrifuged supernatant of nucleoplasmic fraction was designated as the nuclear fraction. The nuclear insoluble fraction was not used in this study, in which chromatin, the membranes of endoplasmic reticulum (ER), Golgi apparatus, and mitochondria might be often involved.

HeLa cells transfected with pFHS-TNRC6A-NES-mut were fractionated, and the localization of TNRC6A-NES-mut was detected by Western blotting using anti-TNRC6A antibody. A successful fractionation of the nucleus (Fig. 2a) and cytoplasm (Fig. 2b) was confirmed by antibodies against α-tubulin, a cytoplasmic marker, and poly (ADP-ribose) polymerase (PARP), a nuclear marker protein. Endogenous TNRC6A signals were detected in the cells transfected with the FHS-tagged empty control vector (pFHS), but no exogenous TNRC6A signals were seen. However, consistent with our previous results [8], TNRC6A-NES-mut was abundant in the nuclear fraction, although a slightly small amount of TNRC6A-NES-mut was observed in the cytoplasmic fraction (Fig. 2a). Contrary to TNRC6A-NES-mut, TNRC6A-NLS-mut protein was predominantly detected in the cytoplasmic fraction (Fig. 2b). We then performed IP using anti-Flag antibody and the nuclear fraction from cells expressing TNRC6A-NES-mut and the cytoplasmic fraction from cells expressing TNRC6A-NLS-mut. TNRC6A-NES-mut protein was successfully immunoprecipitated from the nuclear fraction. In addition, AGO2, a typical TNRC6A-interacting protein, was immunoprecipitated with TNRC6A-NES-mut (Fig. 2c). TNRC6A-NLS-mut was obtained from the cytoplasmic fraction, and the IP of AGO2 was also confirmed (Fig. 2d). Silver staining was performed to detect proteins contained in these immunoprecipitates (Fig. 2e and f). We clearly show that multiple proteins other than AGO protein are contained in both TNRC6A-NES-mut complexes and TNRC6A-NLS-mut complexes.

Identification and classification of proteins co-immunoprecipitated with nuclear and cytoplasmic TNRC6A

Proteins co-immunoprecipitated with TNRC6A-NES-mut from the nuclear fraction or with TNRC6A-NLS-mut from the cytoplasmic fraction were analyzed using nano-liquid chromatography-electrospray ionization-MS/MS. In total, 628 and 522 proteins were identified in association with TNRC6A-NES-mut and TNRC6A-NLS-mut, respectively, and 247 proteins were associated

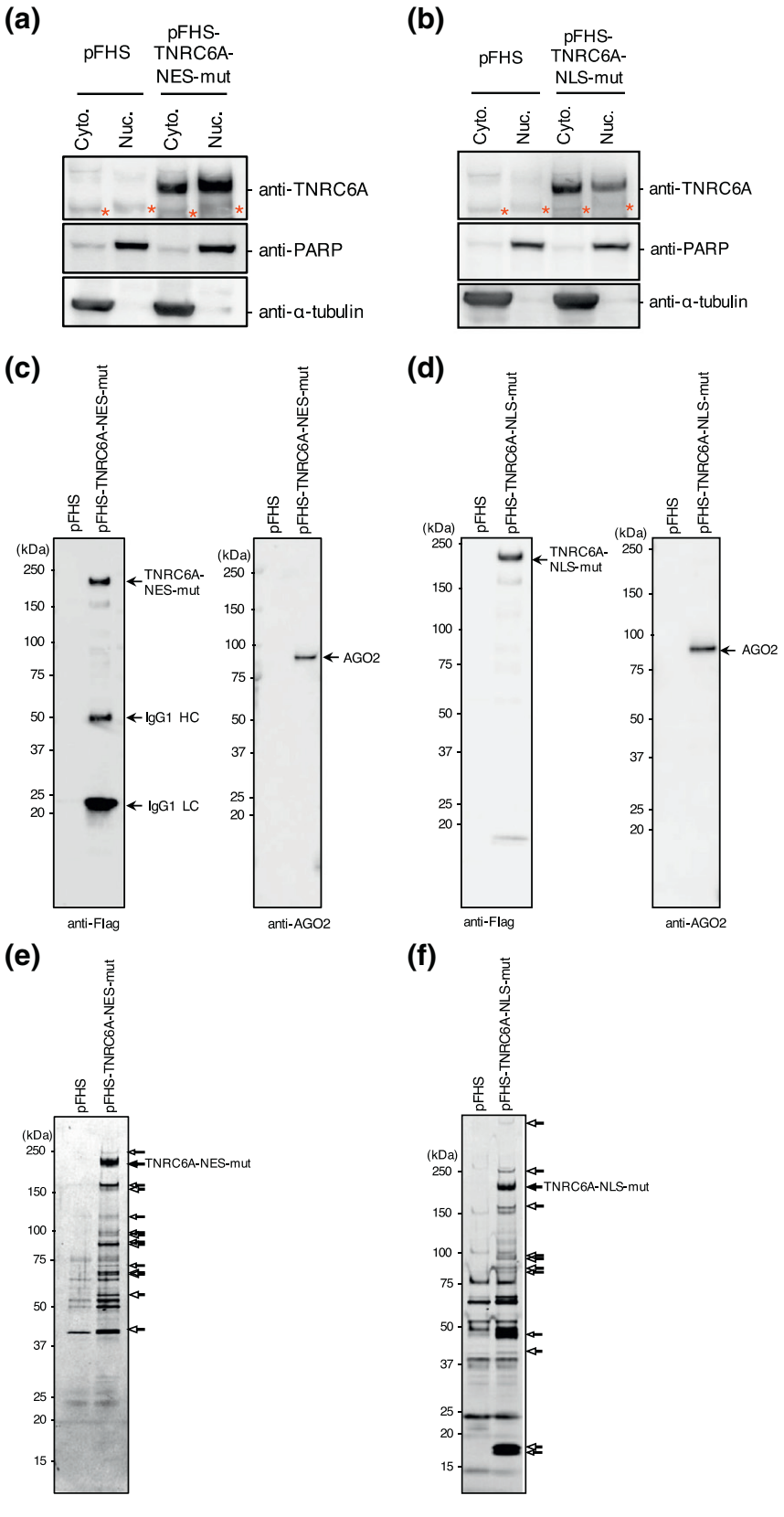

Fig. 2 (*legend on next page*)

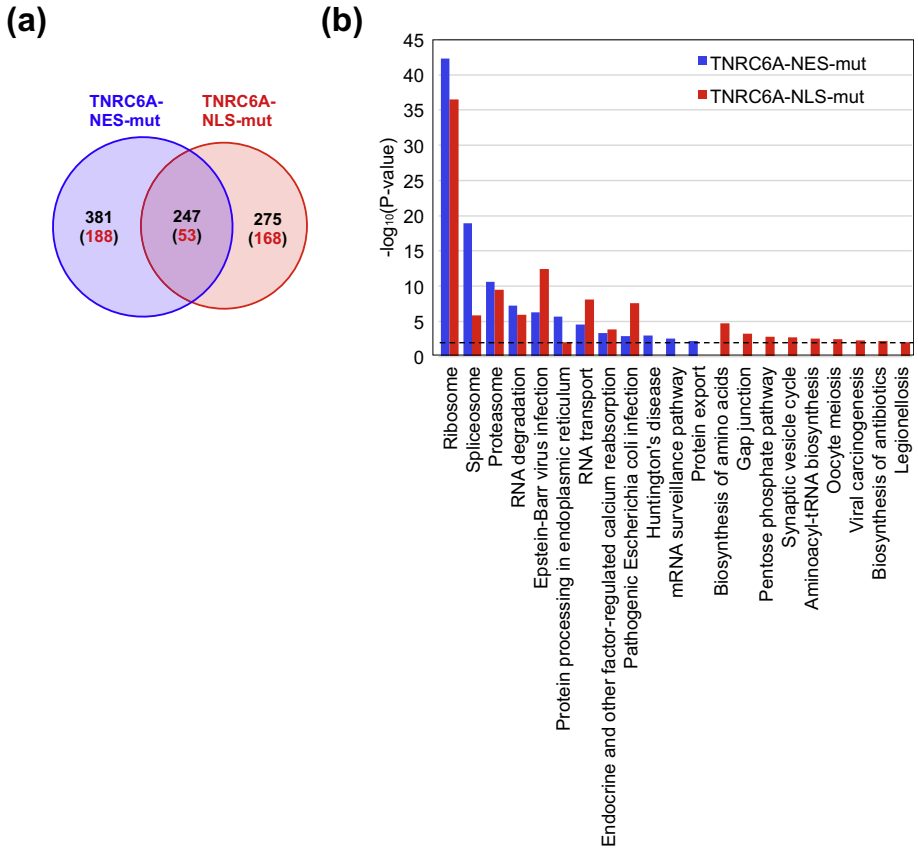

Fig. 3. Results of MS. (a) Venn diagram of immunoprecipitated proteins categorized into the nuclear fraction of TNRC6A-NES-mut, the cytoplasmic fraction of TNRC6A-NLS-mut, and overlapped proteins in both fractions. Black numbers indicate the total number of identified proteins, and red numbers indicate the proteins identified for the first time in this study. Note that the known proteins were identified by the experiments using wild-type TNRC6A-C or AGO1–4 proteins. (b) Classification of identified proteins into KEGG pathways. Blue bars indicate the proteins in the TNRC6A-NES-mut immunoprecipitate, and red bars indicate the proteins in the TNRC6A-NLS-mut immunoprecipitate. The vertical axis indicates $-\log_{10}(P\text{-value})$, then $p < 0.01$ means more than 2.0 (dotted line).

with both (Fig. 3a and Supplementary Tables S1 and S2). Furthermore, 381 and 275 proteins were exclusively associated with TNRC6A-NES-mut and TNRC6A-NLS-mut, respectively. Compared to previously identified proteins associated with TNRC6A-C and AGO1–4 proteins [11–21], 188, 168, and 53 proteins were newly detected in TNRC6A-NES-mut complex, the TNRC6A-NLS-mut complex, and both, respectively.

The identified proteins were classified into possible functional pathways using the Kyoto Encyclopedia of Genes and Genomes (KEGG) database[†] [22] (Fig. 3b and Supplementary Tables S1 and S2). Many nuclear and cytoplasmic proteins immunoprecipitated with TNRC6A were identified in RNA degradation pathway (Fig. 4). The components of CCR4-negative on TATA-less (NOT), poly(A)-binding protein 1, a DEAD-box helicase

Fig. 2. Fractionation and IP of nuclear and cytoplasmic fractions. (a and b) Verification of fractionated samples. pFHS and (a) pFHS-TNRC6A-NES-mut or (b) pFHS-TNRC6A-NLS-mut was transfected into HeLa cells, and cytoplasmic or nuclear fraction was separated. Anti-TNRC6A was used for the detection of TNRC6A, and anti-PARP and anti-α-tubulin were used for nuclear and cytoplasmic markers, respectively. Red asterisks indicate the endogenous TNRC6A protein. (c and d) Western blots of immunoprecipitated fraction with anti-Flag antibody of (c) nuclear fraction of the cells transfected with pFHS-TNRC6A-NES-mut, and (d) cytoplasmic fraction of the cells transfected with pFHS-TNRC6A-NLS-mut. Left panels indicate the results using anti-Flag antibody, and right panels are results using anti-AGO2 antibody. In the left panel of (c), heavy chain (HC) and light chain (LC) of immunoglobulin (IgG) 1 derived from beads were contaminated. (e and f) Silver staining of immunoprecipitated fractions. Immunoprecipitated fractions of the cells transfected with pFHS and (e) pFHS-TNRC6A-NES-mut or (f) pFHS-TNRC6A-NLS-mut. Black arrow indicates TNRC6A-NES-mut or TNRC6A-NLS-mut protein, and white arrows indicate the possible interacting proteins.

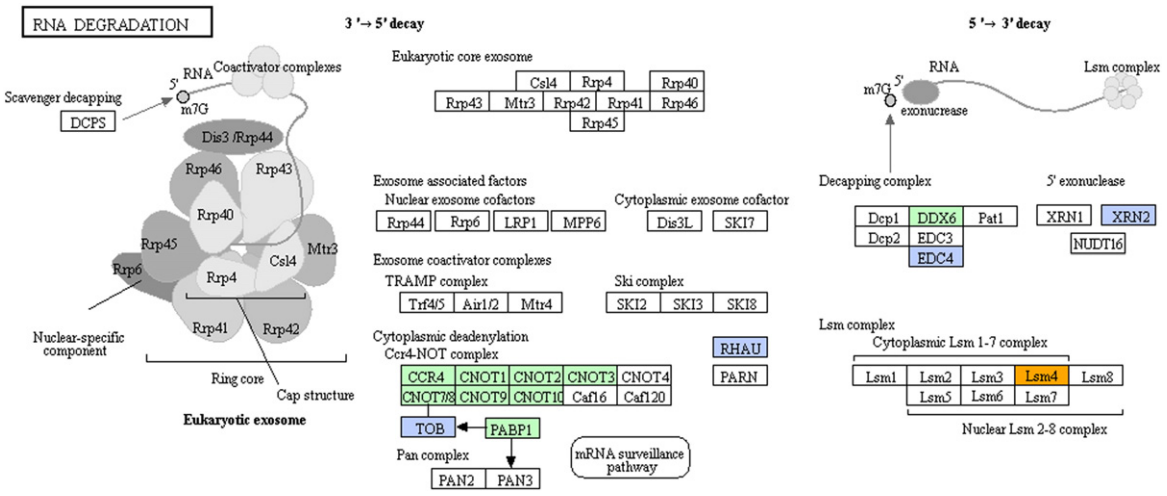

Fig. 4. Identified proteins involved in the KEGG eukaryotic RNA degradation pathway. RNA degradation pathways are classified into two pathways: the 5′ to 3′ decay pathway, which is followed by decapping that permits the 5′ to 3′ exonucleolytic degradation, and the 3′ to 5′ pathway, in which the exosome plays a key role to induce deadenylation. Green indicates the proteins immunoprecipitated with anti-Flag antibody in both nuclear and cytoplasmic fractions. Blue, specific proteins identified in the nuclear fraction. Orange, specific proteins identified in the cytoplasmic fraction.

protein, DDX6 (Rck/p54) [23,24] were commonly found in both nuclear and cytoplasmic fractions (Fig. 4 and Table 1). Furthermore, TOB, whose functions are associated with deadenylase subunits of the CCR4–NOT complex [25], an RNA helicase DHX36 (RNA helicase associated with AU-rich element ARE) [26], EDC4, responsible for mRNA decapping [27], and 5′ to 3′ exonuclease XRN2 [28] were identified in the nuclear fraction, and Sm-like protein 4 involved in mRNA degradation [29] was recovered in the cytoplasmic fraction. Proteins associated with the ribosome pathway were abundant in both the nuclear and cytoplasmic TNRC6A complexes (Fig. 3b). The ribosome pathway proteins usually interact with mRNAs, which directly associate with miRNAs but indirectly associate with AGO or TNRC6A proteins. Thus, many proteins in the ribosomal pathway are thought to be immunoprecipitated by such indirect interactions, and this may be true for other proteins.

Proteins from the spliceosomal pathway were abundantly identified in the nuclear TNRC6A complex (Fig. 3b). Most proteins involved in the small nuclear RNA (snRNA) complexes, containing U1, U2, U2-related, U4, U5, and U6, were identified (Fig. 5 and Table 2). Proteins categorized into protein processing in the ER were also significantly detected (Fig. 3b). Since the nuclear fraction obtained using our fractionation procedure contains ER (Fig. 1c), these proteins were immunoprecipitated with TNRC6A-NES-mut from the nuclear fraction but are not considered to function in the nucleus. In contrast, proteins involved in the Epstein–Barr virus infection, pathogenic *Escherichia coli* infection, and RNA transport pathways were abundant in the cytoplasmic TNRC6A complexes (Fig. 3b). Thus, cytoplasmic TNRC6A may have unidentified functions associated with pathogen infection or RNA transport in the cytoplasm. Proteins associated with Huntington's disease, mRNA surveillance, and protein export pathways were specifically detected in TNRC6A-NES-mut immunoprecipitates, and those associated with the biosynthesis of amino acids, gap junction, pentose phosphate pathway, synaptic vesicle cycle, aminoacyl-tRNA biosynthesis, oocyte meiosis, viral carcinogenesis, biosynthesis of antibiotics, and legionellosis pathways were detected in TNRC6A-NLS-mut immunoprecipitates (Fig. 3b). We cannot yet determine the significance of these results, since only a small population of proteins involved in each pathway were identified.

Verification of the interaction of TNRC6A with immunoprecipitated proteins

To verify the interaction between TNRC6A protein and the immunoprecipitated proteins, we performed the IP experiment for CCR4-NOT subunit proteins, which were classified into RNA degradation pathway and were identified as top-ranked proteins in the immunoprecipitates using both TNRC6A-NES-mut and TNRC6A-NLS-mut (Table 1). The CCR4-NOT complex is a multisubunit complex conserved in sequence and function throughout the eukaryotes and is involved in many functions [30,31], including regulation of gene expression in various processes, from transcription in the nucleus [32,33] to mRNA decay, quality control, translational repression, and protein ubiquitination in the cytoplasm [34,35]. RNA silencing is thought to occur mainly in the cytoplasm

Table 1. Proteins classified into RNA degradation pathway using KEGG database

Bait protein	Protein GI Accession		Description	M.W.	Score
TNRC6A-NES-mut	18860916		5′–3′ exoribonuclease 2	108.51	929.64
	28872722		protein BTG3 isoform b	29.10	143.58
	42716275	•	CCR4-NOT transcription complex subunit 1 isoform a	266.77	10,175.84
	388454220		CCR4-NOT transcription complex subunit 1 isoform c	266.21	10,078.17
	13123772		CCR4-NOT transcription complex subunit 10 isoform 1	82.26	956.21
	7657385	•	CCR4-NOT transcription complex subunit 2	59.70	2353.47
	7657387	•	CCR4-NOT transcription complex subunit 3	81.82	1770.92
	115583679	•	CCR4-NOT transcription complex subunit 6-like	62.96	660.13
	85067507		CCR4-NOT transcription complex subunit 7 isoform 1	32.72	1340.29
	31542315	•	CCR4-NOT transcription complex subunit 8	33.52	692.13
	4885579	•	Cell differentiation protein RCD1 homolog isoform 2	33.61	1218.70
	164664518	•	Probable ATP-dependent RNA helicase DDX6	54.38	564.43
	167830433		Probable ATP-dependent RNA helicase DHX36 isoform 1	114.69	720.90
	45827771		Enhancer of mRNA-decapping protein 4	151.57	38.68
	24234688	•	Stress-70 protein, mitochondrial precursor	73.63	4575.10
	31542947		60-kDa heat shock protein, mitochondrial	61.02	5278.91
	334191701		6-phosphofructokinase type C isoform 2	85.26	278.74
	46367787	•	Polyadenylate-binding protein 1	70.63	3278.55
	208431836	•	Polyadenylate-binding protein 4 isoform 3	69.53	2188.69
	7706739		Protein Tob2	36.61	201.27
TNRC6A-NLS-mut	42716275	•	CCR4-NOT transcription complex subunit 1 isoform a	266.77	2930.45
	376319247		CCR4-NOT transcription complex subunit 10 isoform 2	79.33	156.43
	7657385	•	CCR4-NOT transcription complex subunit 2	59.70	633.15
	7657387	•	CCR4-NOT transcription complex subunit 3	81.82	196.17
	115583679	•	CCR4-NOT transcription complex subunit 6-like	62.96	234.82
	85067505		CCR4-NOT transcription complex subunit 7 isoform 2	28.21	219.58
	31542315	•	CCR4-NOT transcription complex subunit 8	33.52	102.64
	4885579	•	Cell differentiation protein RCD1 homolog isoform 2	33.61	533.02
	164664518	•	Probable ATP-dependent RNA helicase DDX6	54.38	45.47
	355477275		U6 snRNA-associated Sm-like protein LSm4 isoform 2	13.80	53.10
	24234688	•	Stress-70 protein, mitochondrial precursor	73.63	35.49
	48762920		6-phosphofructokinase, liver type	84.96	1006.30
	4505749		6-phosphofructokinase, muscle type isoform 2	85.13	209.28
	11321601		6-phosphofructokinase type C isoform 1	85.54	894.49
	46367787	•	Polyadenylate-binding protein 1	70.63	960.43
	208431836	•	Polyadenylate-binding protein 4 isoform 3	69.53	308.64

The list of proteins co-immunoprecipitated with TNRC6A-NES-mut from nuclear fraction (upper rows) or TNRC6A-NLS-mut from cytoplasmic fraction (lower rows). "Score" indicates the sum of the scores of the unique peptides for that protein based on the calculated probability, *P*, that the observed match between the experimental data and the database sequence is a random event. The numerical value in the score column is −10Log(*P*). Black circles indicate proteins detected in both immunoprecipitates of TNRC6A-NES-mut and TNRC6A-NLS-mut.

by interaction of TNRC6A protein with the CCR4-NOT complex [14,18,36,37]. However, since many components essential for RNA silencing involving CCR4-NOT complex proteins were also detected in the immunoprecipitates in the nuclear fraction, our results suggest that the similar phenomenon involving RNA silencing components is able to occur in the nucleus when TNRC6A is translocated into the nucleus. Among the subunit proteins of the CCR4-NOT complex, seven (CCR4, CNOT1, CNOT2, CNOT3, CNOT7/8, CNOT9, and CNOT10) were commonly immunoprecipitated in both cytoplasmic and nuclear fractions with TNRC6A (Fig. 4 and Table 1). Among them, since the CNOT1 is the largest subunit of the complex and functions as a scaffold protein in the assembly of other components, we used CNOT1 for validation experiment. To clarify the interaction between TNRC6A and CNOT1, we transfected each of pFHS-TNRC6A-WT or pFHS-TNRC6A-NES-mut into HeLa cells. Then, the subcellular localization of CNOT1 and TNRC6A was investigated by western blotting. Since there was a possibility that the nuclear fraction obtained using our cell fractionation procedure contained ER, we modified the procedure to segregate ER fraction from the nuclear fraction using 0.3% NP-40 before lysis of nuclear membrane by 0.5% NP-40 (see Fig. 1c) for validation experiment. Successful fractionation was confirmed by the nuclear marker (anti-PARP), the ER marker (anti-calreticulin), and the cytoplasmic marker (anti-α-tubulin; Fig. 6a). Wild-type TNRC6A protein was preferentially detected in the cytoplasmic fraction by anti-TNRC6A antibody, and the small amount was observed in the nuclear fraction and also in the ER fraction. Although a large amount of TNRC6A with NES mutation was also detected in the cytoplasm, the larger amount of NES mutant protein was apparently observed in the nuclear and ER fractions compared to

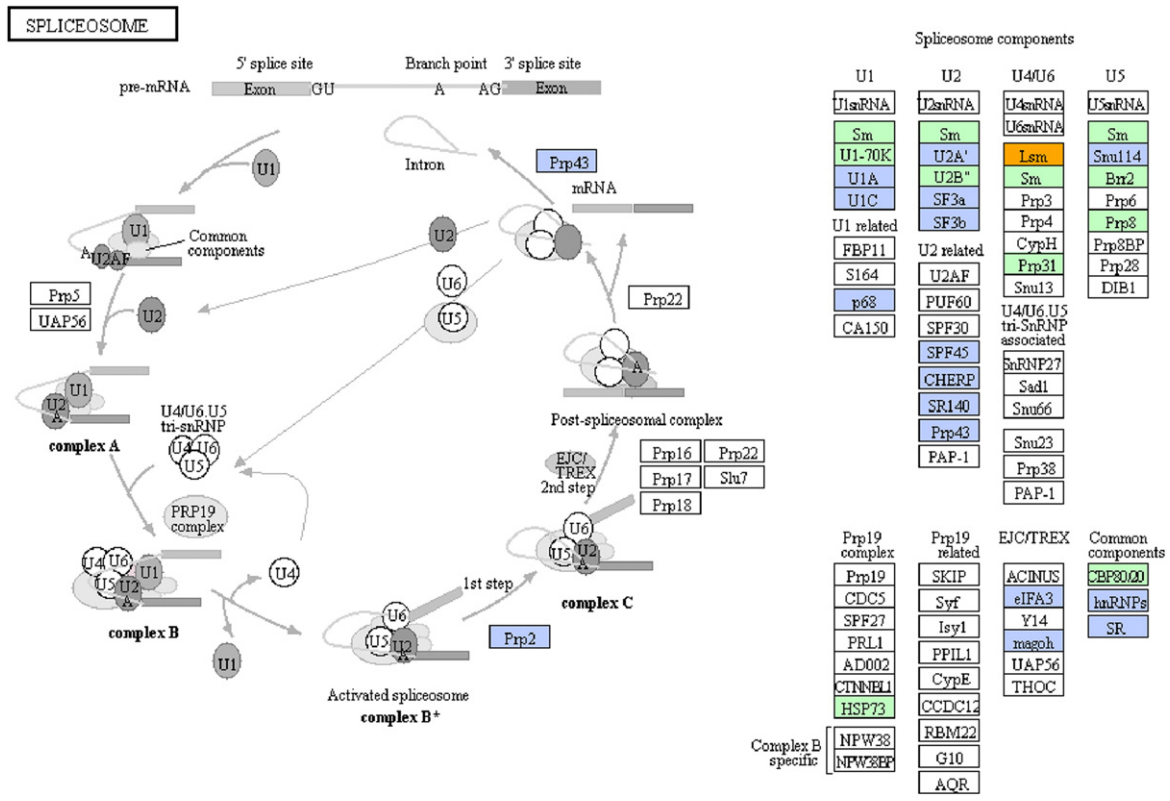

Fig. 5. Identified proteins involved in the KEGG spliceosome pathway. In splicing, introns are excised and exons are joined by the spliceosome components. The spliceosome is usually composed of five snRNPs, U1, U2, U4, U5, and U6 snRNPs, and several spliceosome-associated proteins. Green indicates the spliceosomal proteins immunoprecipitated with anti-Flag antibody in both nuclear and cytoplasmic fractions. Blue, specific proteins identified in the nuclear fraction. Orange, specific proteins identified in the cytoplasmic fraction.

wild-type TNRC6A, suggesting that NES mutant protein preferably translocates from the cytoplasm to the nucleus through ER (Fig. 6a). CNOT1 protein was mainly detected in the cytoplasmic fractions of wild-type TNRC6A and its NES mutant (Fig. 6a), and their amounts were slightly higher in both ER and nuclear fractions from the cells expressing NES mutant of TNRC6A compared to those from the cells expressing wild-type TNRC6A. The essentially similar results were also observed for AGO2 proteins, although the differences in amounts of AGO2 proteins in both nuclear and ER fractions were not so definitive compared to CNOT1. IP using anti-Flag and anti-TNRC6A antibodies revealed that the large amounts of TNRC6A and TNRC6A-NES-mut proteins were located in the cytoplasm, and the amounts of NES mutant proteins were clearly higher in the nucleus and ER fraction compared to those of wild-type TNRC6A (Fig. 6b). CNOT1 was co-immunoprecipitated with wild-type TNRC6A and its NES mutant in the cytoplasm, and the amount of co-immunoprecipitated CNOT1 with TNRC6A-NES-mut protein was higher than that with wild-type TNRC6A protein in both nuclear and ER fractions. Thus, it was suggested that the cytoplasmic CNOT1 was translocated into the nucleus through ER, associating with TNRC6A. The clear differences in the amounts of AGO2 proteins co-immunoprecipitated with wild-type TNRC6A or TNRC6A-NES-mut protein were undetermined.

Discussion

We have previously revealed that TNRC6A is a protein that shuttles between the cytoplasm and nucleus [8]. The components involved in the nuclear and cytoplasmic TNRC6A complexes were identified for the first time in this study using TNRC6A-NES-mut and TNRC6A-NLS-mut. Our results revealed that many proteins involved in the RNA degradation pathway were immunoprecipitated with TNRC6A in both the cytoplasmic and nuclear fractions (Fig. 3b and Table 1). TNRC6A also interacts with many distinct proteins between the nucleus and cytoplasm.

To verify the MS results, we examined the interaction between TNRC6A and CNOT1. Multiple

Table 2. Proteins classified into spliceosome pathway using KEGG database

Bait protein	Protein GI Accession		Description	M.W.	Score
TNRC6A-NES-mut	4758138		Probable ATP-dependent RNA helicase DDX5	69.1	278.81
	68509926		Putative pre-mRNA-splicing factor ATP-dependent RNA helicase DHX15	90.88	526.73
	256000749		Putative pre-mRNA-splicing factor ATP-dependent RNA helicase DHX16 isoform 2	112.38	101.21
	14249678		Splicing factor 45	44.93	90.63
	56699409		RNA-binding motif protein, X chromosome isoform 1	42.31	361.74
	122937227		U2 snRNP-associated SURP motif-containing protein	118.22	85.48
	119226260		Calcium homeostasis ER protein	103.64	36.42
	217272894		116-kDa U5 small nuclear ribonucleoprotein component isoform b	105.32	122.29
	7661920		Eukaryotic initiation factor 4A–III	46.84	474.39
	194248072	•	Heat shock 70-kDa protein 1A/1B	70.01	2170.98
	5729877	•	Heat shock cognate 71-kDa protein isoform 1	70.85	3465.38
	4504445		Heterogeneous nuclear ribonucleoprotein A1 isoform a	34.18	359.30
	117190174	•	Heterogeneous nuclear ribonucleoproteins C1/C2 isoform b	32.32	652.68
	14165435	•	Heterogeneous nuclear ribonucleoprotein K isoform b	50.94	2037.89
	157412270	•	Heterogeneous nuclear ribonucleoprotein M isoform b	73.57	2191.56
	14141161	•	Heterogeneous nuclear ribonucleoprotein U isoform b	88.92	1041.53
	4505087		Protein mago nashi homolog	17.15	78.71
	4505343	•	Nuclear cap-binding protein subunit 1	91.78	516.72
	222352151	•	Poly(rC)-binding protein 1	37.47	205.97
	221136939	•	U4/U6 small nuclear ribonucleoprotein Prp31	55.42	2260.59
	91208426	•	Pre-mRNA-processing-splicing factor 8	273.43	27.54
	4506901		Serine/arginine-rich splicing factor 3	19.32	27.21
	5902102	•	Small nuclear ribonucleoprotein Sm D1	13.27	436.53
	4759158	•	Small nuclear ribonucleoprotein Sm D2 isoform 1	13.52	67.91
	4,759,160	•	Small nuclear ribonucleoprotein Sm D3	13.91	136.12
	29568103	•	U1 small nuclear ribonucleoprotein 70 kDa	51.53	62.65
	40217847	•	U5 small nuclear ribonucleoprotein 200-kDa helicase	244.35	224.12
	50593002		U2 small nuclear ribonucleoprotein A′	28.40	76.19
	4759156		U1 small nuclear ribonucleoprotein A	31.26	206.91
	38149981	•	U2 small nuclear ribonucleoprotein B″	25.47	192.53
	4507127		U1 small nuclear ribonucleoprotein C	17.38	46.04
	4507131		Small nuclear ribonucleoprotein F	9.72	58.88
	4507125	•	Small nuclear ribonucleoprotein-associated proteins B and B′ isoform B	23.64	74.94
	5803167		Splicing factor 3A subunit 3	58.81	73.60
	54112117		Splicing factor 3B subunit 1 isoform 1	145.74	584.47
	55749531		Splicing factor 3B subunit 2	100.16	451.78
	54112121	•	Splicing factor 3B subunit 3	135.49	629.54
	5032069		Splicing factor 3B subunit 4	44.36	114.02
	7706326		Pre-mRNA branch site protein p14	14.58	320.92
	345197228		Transformer-2 protein homolog beta isoform 2	21.92	169.02
TNRC6A-NLS-mut	355477275		U6 snRNA-associated Sm-like protein LSm4 isoform 2	13.80	53.10
	194248072	•	Heat shock 70-kDa protein 1A/1B	70.01	2170.98
	13676857		Heat shock-related 70-kDa protein 2	69.98	1111.41
	5729877	•	Heat shock cognate 71-kDa protein isoform 1	70.85	3465.38
	117190174	•	Heterogeneous nuclear ribonucleoproteins C1/C2 isoform b	32.32	652.68
	14165435	•	Heterogeneous nuclear ribonucleoprotein K isoform b	50.94	2037.89
	157412270	•	Heterogeneous nuclear ribonucleoprotein M isoform b	73.57	2191.56
	14141161	•	Heterogeneous nuclear ribonucleoprotein U isoform b	88.92	1041.53
	4505343	•	Nuclear cap-binding protein subunit 1	91.78	516.72
	222352151	•	Poly(rC)-binding protein 1	37.47	205.97
	221136939	•	U4/U6 small nuclear ribonucleoprotein Prp31	55.42	2260.59
	91208426	•	Pre-mRNA-processing-splicing factor 8	273.43	27.54
	5902102	•	Small nuclear ribonucleoprotein Sm D1	13.27	436.53
	4759158	•	Small nuclear ribonucleoprotein Sm D2 isoform 1	13.52	67.91
	4759160	•	Small nuclear ribonucleoprotein Sm D3	13.91	136.12
	29568103	•	U1 small nuclear ribonucleoprotein 70 kDa	51.53	62.65
	40217847	•	U5 small nuclear ribonucleoprotein 200-kDa helicase	244.35	224.12
	38149981	•	U2 small nuclear ribonucleoprotein B″	25.47	192.53
	4507129		Small nuclear ribonucleoprotein E	10.80	28.70
	4507125	•	Small nuclear ribonucleoprotein-associated proteins B and B′ isoform B	23.64	74.94
	54112121	•	Splicing factor 3B subunit 3	135.49	629.54

The list of proteins co-immunoprecipitated with TNRC6A-NES-mut from nuclear fraction (upper rows) or TNRC6A-NLS-mut from cytoplasmic fraction (lower rows). "Score" indicates the sum of the scores of the unique peptides for that protein based on the calculated probability, *P*, that the observed match between the experimental data and the database sequence is a random event. The numerical value in the score column is –10Log(*P*). Black circles indicate proteins detected in both immunoprecipitates of TNRC6A-NES-mut and TNRC6A-NLS-mut.

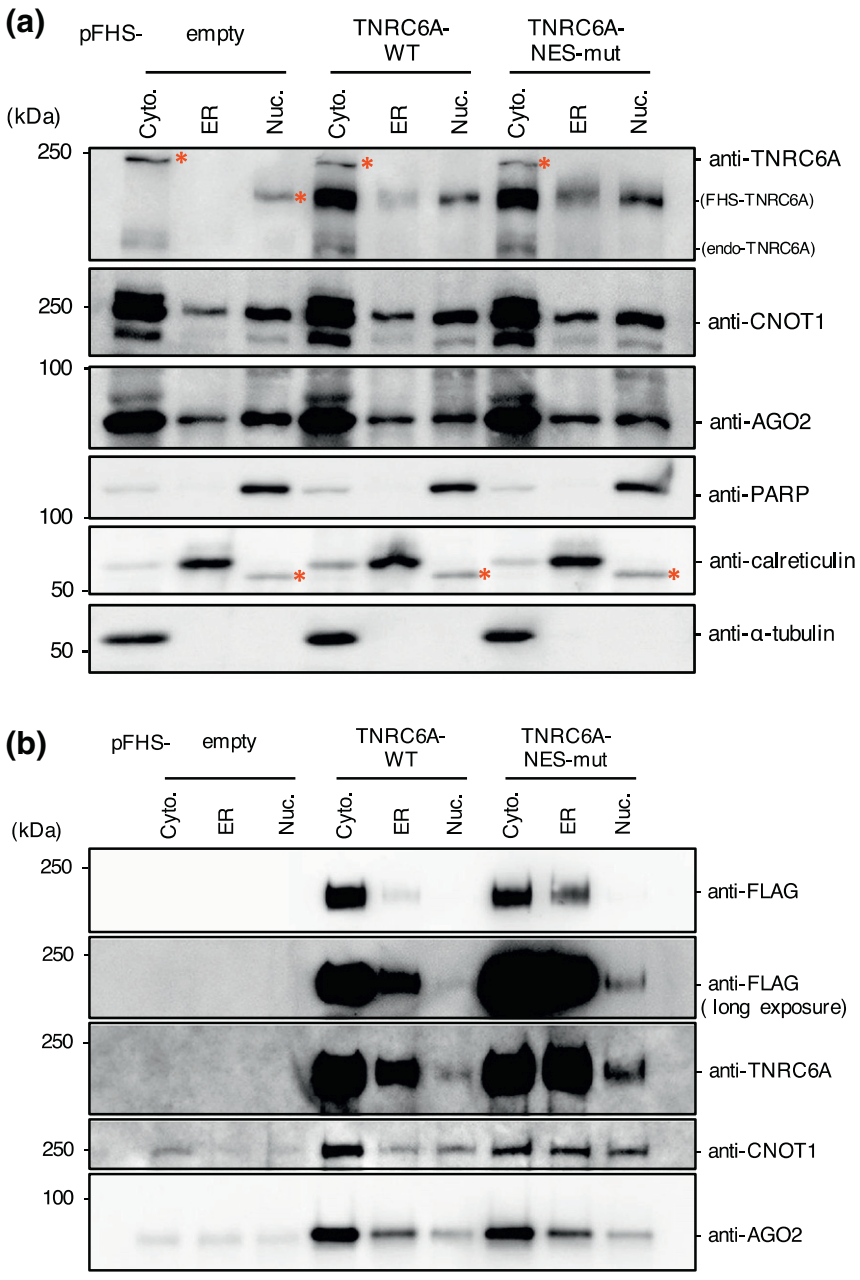

Fig. 6. Verification of the result of MS using CNOT1. (a) Subcellular localization examined by the modified cell fractionation procedure, which separates cells into nuclear, ER, and cytoplasmic fractions. The cells transfected with pFHS, pFHS-TNRC6A-WT, or pFHS-TNRC6A-NES-mut were used. TNRC6A protein was detected by anti-TNRC6A antibody. CNOT1, anti-CNOT1 antibody. AGO2, anti-AGO2 antibody. PARP was used as a nuclear marker and detected by anti-PARP antibody. Calreticulin, an ER marker, anti-calreticulin antibody. α-tubulin, a cytoplasmic marker, anti-α-tubulin antibody. Red asterisks indicate nonspecific bands. (b) Immunoprecipitation using the nuclear, ER, and cytoplasmic fractions of the cells transfected with pFHS, pFHS-TNRC6A-WT, or pFHS-TNRC6A-NES-mut. Immunoprecipitation was carried out using anti-Flag antibody, and TNRC6A, CNOT1, and AGO2 proteins were detected. The experiments were performed two times, and the typical results were shown.

subunit proteins contained in the CCR4-NOT complex were significantly immunoprecipitated with TNRC6A-NES-mut and TNRC6A-NLS-mut protein (Table 1). When pFHS-TNRC6A-WT was transcfected into HeLa cells, both TNRC6A and CNOT1 were mainly observed in the cytoplasm, and small amounts were in the nucleus (Fig. 6a). Thus, these proteins are able to shuttle between cytoplasm and nucleus but are preferably localized in the cytoplasm in the normal condition of HeLa cells. However,

pFHS-TNRC6A-NES-mut was transfected, and the amounts of CNOT1 protein co-immunoprecipitated with NES-mut in the nucleus and ER fractions evidently increased (Fig. 6b). Thus, it was strongly suggested that CNOT1 is recruited from cytoplasm to nucleus through ER by interacting with TNRC6A. In addition to the CCR4-NOT complex components, PABP, which plays an important role in RNA silencing by interacting with CNOT1 [38,39], and DDX6 (Rck/p54) that functions in mRNA decapping [23,24], were also found in both nuclear and cytoplasmic immunoprecipitates. Furthermore, TOB, RHAU, EDC4, and XRN2 were identified among the TNRC6A-associating proteins in the nucleus. TOB interacts with deadenylase subunits of the CCR4-NOT complex [25], RHAU is an RNA helicase DHX36 that is necessary for deadenylation [26], and EDC4 (also known as Hedls, Ge-1, or RCD-8) enhances mRNA decapping [27]. XRN2 is a 5′ to 3′ exonuclease [28], and Sm-like protein 4 is associated with mRNA degradation [29]. Thus, these results strongly suggest that the some unknown mechanism using RNA silencing components is induced via TNRC6A in the nucleus as RNA silencing in the cytoplasm. The isoforms of immunoprecipitated proteins in the nucleus and the cytoplasm were not necessarily the same. The isoforms of CNOT1, CNOT7, and CNOT10 differed between the nucleus and cytoplasm (Table 1). The isoforms of CNOT1, CNOT7, and CNOT10 immunoprecipitated with the nuclear TNRC6A-NES-mut were CNOT1 isoform c, CNOT7 isoform 1, and CNOT10 isoform 1. Isoforms immunoprecipitated with cytoplasmic TNRC6A-NLS-mut included CNOT7 isoform 2 and CNOT10 isoform 2. The common isoform a of CNOT1 was found in both fractions. CNOT1 is the largest subunit of the CCR4-NOT complex and functions as a scaffold protein in the assembly of other components. The N-terminal region of CNOT1 interacts with CNOT11, which interacts with CNOT10 [40]; the middle region directly interacts with CNOT7 or CNOT8 [40–42]; and the C-terminal region interacts with CNOT2/CNOT3 [40,43]. Thus, the isoforms of CNOT1, CNOT7, and CNOT10 are important subunits. CNOT7 and CNOT8 are paralogous genes, known as hCAF1a and hCAF1b, respectively. The hCAF1z isoform complex differs from the conventional CCR4-NOT deadenylase complex [44] and is concentrated in nuclear Cajal bodies shuttling between the nucleus and cytoplasm. It subjects substrate RNAs to rapid deadenylation and slow exonucleolytic degradation from the 3′ end *in vitro*. It is possible that such functional changes also occur via the nuclear and the cytoplasmic isoforms of CNOT1, CNOT7, and CNOT10.

Proteins involved in the spliceosome pathway were identified in the nuclear fraction of cells expressing TNRC6A-NES-mut protein, and those involved in the Epstein–Barr virus infection, RNA transport, and pathogenic *E. coli* infection pathways were detected in the cytoplasmic fraction of the cells expressing TNRC6A-NLS-mut. Thus, it is possible that TNRC6A has various other roles in the nucleus and the cytoplasm in addition to RNA silencing: the splicing in the nucleus and pathogenic infection or RNA transport in the cytoplasm. Many proteins involved in the splicing machinery were detected in the nuclear fraction. Most components of snRNA complexes containing U1, U2, U2-related, U4/U6, U5, exon junction complex/transcription export complex, and common components of the spliceosome were identified (Fig. 5 and Table 2). Some of these components were detected in both the cytoplasmic and nuclear fractions, because snRNAs shuttle between the nucleus and cytoplasm [45].

It has been reported that vertebrate (TNRC6A/B/C) and insect GW182 proteins share a common domain organization characterized by two annotated structural domains: a central UBA-like domain and a C-terminal RRM [5], and NES is positioned in the UBA-like domain. Although these domains are embedded in regions predicted to be unstructured, it might be possible that the mutations in NES change the structure of TNRC6A and the interacting proteins. However, in the validation experiment, we revealed that CNOT1 protein was able to be co-immunoprecipitated with wild-type TNRC6A, although the co-immunoprecipitated amount of wild-type TNRC6A protein was smaller compared to TNRC6A with NES mutation (Fig. 6b). Thus, at least CNOT1 can interact with TNRC6A even when its NES was mutated.

It is clear that AGO proteins also regulate nuclear processes in association with small RNAs [46]. In *Schizosaccharomyces pombe*, AGOs participate in the assembly of heterochromatin at centromeric regions via histone methylation [47]. Also, in mammalian cells, AGO1 and/or AGO2, in association with small RNAs complementary to genomic regions, repress [48,49] or activate gene expression [50,51] and control alternative splicing [11,52] and DNA double-strand break repair [53,54]. Although it is unclear how AGO2 translocates into the nucleus, importin 8, a member of the karyopherin β family, mediates the cytoplasm-to-nuclear transport of mature miRNAs with help from the AGO2 complex [16,55]. Our MS and Western blot did not discriminate whether the splicing is regulated by AGO or TNRC6A directly.

In most cells, TNRC6A is mainly observed in the cytoplasm, even though it can shuttle between the cytoplasm and the nucleus. However, TNRC6A is mainly localized in the nucleus in several human cancers, such as gastric, colorectal, prostate, and esophageal cancers [9,10]. In this study, we revealed that TNRC6A protein interacts with CNOT1 in the nucleus. Human CNOT1 protein is known to recruit other CCR4-NOT subunits into the nucleus and

function as a transcriptional repressor of nuclear estrogen receptor α in hormone-dependent fashion [33]. Furthermore, the depletion of endogenous CNOT1 in breast cancer cells results in the deregulation of endogenous estrogen receptor α target genes. Thus, TNRC6A may be important for the understanding of molecular mechanism involved in various cancers containing breast cancer.

Materials and Methods

Cell culture and transfection

HeLa cells derived from human cervical cancer were cultured in Dulbecco's modified Eagle's medium (Wako) supplemented with 10% fetal bovine serum (GIBCO) and antibiotics [Penicillin–Streptomycin Solution (×100; Wako)] at 37 °C in 5% CO_2.

Cells were seeded at 2.0×10^6 cells/ml into each of 90-mm dishes 1 day before transfection. Transfection was performed using Polyethylenimine "MAX" (Polyscience Inc.) with 10 μg of total plasmid DNA per dish according to the manufacturer's protocol.

Cell fractionation

Cells were lysed in ice-cold lysis buffer [10 mM Hepes-NaOH (pH 7.9), 1.5 mM $MgCl_2$, 10 mM KCl, 50 mM NaCl, 0.5 mM DTT, 1 mM EDTA, 1 mM Na_3Vo_4, 10 mM NaF, and 1 x complete protease inhibitor cocktail (Roche)] supplemented with digitonin (130 μg/1.0×10^7 cells). After incubation for 10 min on ice, cells were centrifuged and supernatant was used as cytoplasmic fraction. Precipitated nuclei were washed two times with ice-cold lysis buffer. To make nuclear extract, we resuspended nuclei in nuclear lysis buffer (same as ice-cold lysis buffer but we increased 50 mM NaCl to 140 mM NaCl and added 0.5% NP40). After incubation for 10 min on ice, cells were centrifuged and supernatant was used as nuclear fraction.

For the experiment in Fig. 6a and b, cells were lysed in ice-cold lysis buffer supplemented with digitonin (130 μg/1.0×10^7 cells). After incubation for 10 min on ice, cells were centrifuged and supernatant was used as cytoplasmic fraction. Precipitates were washed with ice-cold lysis buffer. To isolate ER fraction, we washed the precipitate three times in ice-cold lysis buffer with 50 mM NaCl with 0.3% NP-40, and the first supernatant was recovered as ER fraction. Then, to make nuclear extract, we resuspended nuclei in high salt nuclear lysis buffer (same as ice-cold lysis buffer but we increased 50 mM NaCl to 420 mM NaCl and added 0.5% NP40). After incubation for 10 min on ice, cells were centrifuged and supernatant was diluted by the addition of two volumes of diluted buffer (same as ice-cold lysis buffer without 50 mM NaCl) and used as nuclear fraction.

IP for MS

For MS analysis, IP of nuclear TNRC6A complexes was performed using HeLa nuclear fraction transfected with pFHS-TNRC6A-NES-mut or pFHS as a control. IP of cytoplasmic TNRC6A complexes was performed using HeLa cytoplasmic fraction transfected with pFHS-TNRC6A-NLS-mut or pFHS. Each extract was centrifuged at 48,000*g* for 30 min at 4 °C, and the supernatant was precleared using Sepharose 4B (Sigma, 4B200), rotating for 1 h at 4 °C. Extracts were transferred to 60 μl of anti-FLAG M2 affinity gel (Sigma, A2220) and incubated with rotation for 2 h at 4 °C. The affinity gel was washed twice with wash buffer (same as ice-cold lysis buffer but we increased 50 mM NaCl to 300 mM NaCl), once with nuclear lysis buffer wash, and twice with TBS buffer [10 mM Tris–HCl (pH 7.5) and 150 mM NaCl]. The bound proteins to the affinity gel were eluted with 50 μl TBS containing 1 mg/ml Flag peptide (Sigma, F-3290), with shaking for 1 h at 4 °C. The eluates were separated from the gel by centrifugation at 800*g* for 2 min at 4 °C. An aliquot of the eluate was subjected to SDS-PAGE, and co-immunoprecipitated proteins were stained using a Silver Stain II kit (Wako).

MS analysis

The remained eluate was digested with trypsin desalted using ZipTipC18 (Millipore) and centrifuged in a vacuum concentrator. Shotgun proteomic analyses by a linear ion trap-orbitrap MS (LTQ-Orbitrap Velos; Thermo Fisher Scientific) coupled with a nanoflow liquid chromatography system (Dina-2A; KYA Technologies) were performed following the previous report [56]. Briefly, trypsinized peptides were injected into a 75-μm reversed-phase C18 column at a flow rate of 10 μl/min. Elution was performed with a linear gradient of solvent A (2% acetonitrile and 0.1% formic acid in H_2O) to solvent B (40% acetonitrile and 0.1% formic acid in H_2O) at 300 nl/min. Peptides were sequentially sprayed from a nanoelectrospray ion source (KYA Technologies) and analyzed by collision-induced dissociation using full-scan MS spectra (from *m*/*z* 380 to 2000). The analyses were carried out in a data-dependent mode. The 20 most intense ions at a threshold level above 2000 were fragmented in the linear ion trap. The orbitrap analyzer was operated to perform shotgun detection with high accuracy. Protein identification was conducted using MS and MS/MS data against a comprehensive, integrated, non-redundant, and well-annotated set of reference sequence including genomic, transcript, and protein of the National Center for Biotechnology Information using Mascot version 2.4.1 (Matrix Science). A maximum of two missed cleavages was allowed, while the mass tolerance was set to 3 ppm for

peptide masses and 0.8 Da for MS/MS peaks, and we applied a filter to satisfy a false discovery rate lower than 1%.

Western blot

The samples were mixed with same volume of 2 x SDS-PAGE sample buffer [4% (wt/vol) SDS, 0.1 M Tris–HCl (pH 6.8), 12% (vol/vol) β-mercaptoethanol, 20% (wt/vol) glycerol, and 0.01% (wt/vol) bromophenol blue], boiled for 5 min, and separated by SDS-PAGE. The gels were transferred to PVDF membrane using a Trans-Blot Turbo Transfer System (Bio-Rad). The membranes were blocked for 1 h at room temperature with 5% skim milk in TBST [20 mM Tris–HCl (pH 7.5), 150 mM NaCl, and 0.1% Tween-20].

Blocked membranes were incubated with the following primary antibodies at 4 °C overnight in TBST + 5% skim milk: anti-Ago2 at 1:500 dilution (Wako, 015–22,031), anti-GW182 (TNRC6A) at 1:2000 (Bethyl Laboratoried, A302-329A), anti-alpha tubulin at 1:1000 (Sigma, T9026), anti-PARP at 1:2000 (Abcam, ab32071), anti-Flag at 1:500 (Sigma, F1804), anti-GFP at 1:2000 (Clontech, 632,592), and anti-CNOT1 at 1:1000 (Proteintech, 14,276–1-AP).

After primary antibody incubation, the membranes were washed three times for 10 min at room temperature with TBST and then incubated for 1 h at room temperature with horseradish peroxidase-conjugated anti-mouse IgG (GE Healthcare, NA931V) at 1:6000 or anti-rabbit IgG (GE Healthcare, NA934V) at 1:6000 in TBST. After being washed three times for 10 min in TBST at room temperature, the membrane was incubated with ECL Prime Western Blotting Detection Reagent (GE Healthcare, RPN2232), and signals were detected by an ImageQuant LAS 4000 (GE Healthcare).

Data analysis of MS

For the classification of identified proteins by MS analysis, the database for annotation, visualization, and integrated discovery was used [57,58]. Accession numbers allocated to each protein were pasted into functional annotation tool (step 1), selected in PROTEIN_GI_ACCESSION (step 2) and Gene List (step 3), and then submitted (step 4). Significantly enriched pathways in KEGG database tested by the modified Fisher's exact test were listed in Fig. 3b, and pathway maps were shown in Figs. 4 and 5.

IP for validation

Cells were seeded at 2.0×10^6 cells/ml into each of 90-mm dishes 1 day before transfection. Then, 10 μg of pFHS, pFHS-TNRC6A-WT, or pFHS-TNRC6A-NES-mut was transfected into HeLa cells. We harvested the cells 2 days after transfection, and cell fractionation into cytoplasm, ER, and nuclear fractions was carried out. Each fraction was centrifuged at 48,000*g* for 30 min at 4 °C, and the supernatant was precleared using Sepharose 4B, rotating for 1 h at 4 °C. Extracts were transferred to 20 μl of anti-Flag M2 affinity gel and incubated with rotation for 2 h at 4 °C. The affinity gel was washed three times with nuclear lysis buffer and resuspended in 30 μl of 2 x SDS-PAGE sample buffer. We boiled the beads for 5 min and separated it by SDS-PAGE.

Fluorescence microscopy

Immunofluorescence was essentially performed as previously reported [8]. Briefly, HeLa cells transfected with various FHS-tagged TNRC6A expression constructs were cultured on 12-well culture plate with a 15-mm glass at the bottom. Cells were fixed with 4% paraformaldehyde and then permeabilized with 0.2% Triton X-100. Cells were incubated with the anti-HA tag monoclonal antibody (MBL, M180–3, 1:800 dilution) in PBS and washed. Then, they were incubated with the Cy3-labeled goat anti-mouse IgG (Amersham biosciences, PA43002, 1:800 dilution) and washed again. They were mounted with DAPI (Invitrogen, P36931) and observed under Zeiss Axiovert 200 fluorescence microscope.

Acknowledgments

We thank Dr. Akira Yasui for kindly providing antibodies. This work was supported by the grants from the Ministry of Education, Culture, Sports, Science and Technology of Japan (21310123, 21115004, 15H04319, and 16H14640) and the grants provided from Suzuken Memorial Foundation to K.U.-T.

Author contributions: K.U.-T. designed the study, and M.S., K.N., and K.U.-T. discussed the procedures and results. M.S. and K.N. prepared the mass spectrometry samples, and H.K.-H. and M.O. performed mass spectrometry. M.S. performed data analysis, and M.S. and K.N. carried out validation experiments. The manuscript was drafted by K.U.-T., and M.S. and K.U.-T. completed the manuscript. All authors read and approved the final manuscript.

Conflict of interest: The authors declare no competing financial interests.

Appendix A. Supplementary Data

Supplementary data to this article can be found online at http://dx.doi.org/10.1016/j.jmb.2017.04.017.

Received 28 December 2016;
Received in revised form 18 April 2017;
Accepted 24 April 2017
Available online 3 May 2017

Keywords:
GW182;
TNRC6A;
mass spectrometry;
RNA degradation;
spliceosome

†http://www.genome.jp/kegg/pathway.html

Abbreviations used:
TNRC6A, trinucleotide repeat-containing gene 6A protein; Q-rich, glutamine-rich; RRM, RNA recognition motif; AGO, Argonaute; miRNA, microRNA; CCR4, carbon catabolite repression 4; CAF1, CCR4-associated factor 1; NLS, nuclear localization signal; NES, nuclear export signal; IP, immunoprecipitation; MS, mass spectrometry; UBA, ubiquitin-associated; FHS, Flag-, HA-, and streptavidin-binding peptide; DAPI, 4′-6-diamidino-2-phenylindole; pFHS-TNRC6A-WT, wild-type FHS-tagged TNRC6A expression construct; TNRC6A-NES-mut, TNRC6A with a NES mutation; TNRC6A-NLS-mut, TNRC6A with an NLS mutation; ER, endoplasmic reticulum; PARP, poly(ADP-ribose) polymerase; KEGG, Kyoto Encyclopedia of Genes and Genomes; NOT, negative on TATA-less; snRNA, small nuclear RNA; RHAU, RNA helicase associated with AU-rich element ARE.

References

[1] T. Eystathioy, E.K.L. Chan, S.A. Tenenbaum, J.D. Keene, K. Griffith, M.J. Fritzler, A phosphorylated cytoplasmic autoantigen, GW182, associates with a unique population of human mRNAs within novel cytoplasmic speckles, Mol. Biol. Cell 13 (2002) 1338–1351.
[2] L. Ding, A. Spencer, K. Morita, M. Han, The developmental timing regulator AIN-1 interacts with miRISCs and may target the argonaute protein ALG-1 to cytoplasmic P bodies in *C. elegans*, Mol. Cell 19 (2005) 437–447.
[3] L. Zhang, L. Ding, T.H. Cheung, M.Q. Dong, J. Chen, A.K. Sewell, X. Liu, J.R. Yates III, M. Han, Systematic identification of *C. elegans* miRISC proteins, miRNAs, and mRNA targets by their interactions with GW182 proteins AIN-1 and AIN-2, Mol. Cell 28 (2007) 598–613.
[4] M.D. Schneider, N. Najand, S. Chaker, J.M. Pare, J. Haskins, S.C. Hughes, T.C. Hobman, J. Locke, A.J. Simmonds, Gawky is a component of cytoplasmic mRNA processing bodies required for early *Drosophila* development, J. Cell Biol. 174 (2006) 349–358.
[5] A. Eulalio, F. Tritschler, E. Izaurralde, The GW182 protein family in animal cells: new insights into domains required for miRNA-mediated gene silencing, RNA 15 (2009) 1433–1442.
[6] D. Baillat, R. Shiekhattar, Functional dissection of the human TNRC6 (GW182-related) family of proteins, Mol. Cell. Biol. 29 (2009) 4144–4155.
[7] C.Y. Chen, D. Zheng, Z. Xia, A.B. Shyu, Ago-TNRC6 triggers microRNA-mediated decay by promoting two deadenylation steps, Nat. Struct. Mol. Biol. 16 (2009) 1160–1166.
[8] K. Nishi, A. Nishi, T. Nagasawa, K. Ui-Tei, Human TNRC6A is an Argonaute-navigator protein for microRNA-mediated gene silencing in the nucleus, RNA 19 (2013) 17–35.
[9] M.S. Kim, J.E. Oh, Y.R. Kim, S.W. Park, M.R. Kang, S.S. Kim, C.H. Ahn, N.J. Yoo, S.H. Lee, Somatic mutations and losses of expression of microRNA regulation-related genes AGO2 and TNRC6A in gastric and colorectal cancers, J. Pathol. 221 (2010) 139–146.
[10] N.J. Yoo, S.Y. Hur, M.S. Kim, J.Y. Lee, S.H. Lee, Immunohistochemical analysis of RNA-induced silencing complex-related proteins AGO2 and TNRC6A in prostate and esophageal cancers, APMIS 118 (2010) 271–276.
[11] M. Ameyar-Zazoua, C. Rachez, M. Souidi, P. Robin, L. Fritsch, R. Young, N. Morozova, R. Fenouil, N. Descostes, J.C. Andrau, J. Mathieu, A. Hamiche, A. Ait-Si-Ali, C. Muchardt, E. Batsche, A. Harel-Bellan, Argonaute proteins couple chromatin silencing to alternative splicing, Nat. Struct. Mol. Biol. 19 (2012) 998–1004.
[12] G. Meister, M. Landthaler, L. Peters, P.Y. Chen, H. Urlaub, R. Luhrmann, T. Tuschl, Identification of novel argonaute-associated proteins, Curr. Biol. 15 (2005) 2149–2155.
[13] J. Hock, L. Weinmann, C. Ender, S. Rudel, E. Kremmer, M. Raabe, H. Urlaub, G. Meister, Proteomic and functional analysis of Argonaute-containing mRNA–protein complexes in human cells, EMBO Rep. 8 (2007) 1052–1060.
[14] M. Chekulaeva, H. Mathys, J.T. Zipprich, J. Attig, M. Colic, R. Parker, W. Filipowicz, miRNA repression involves GW182-mediated recruitment of CCR4-NOT through conserved W-containing motifs, Nat. Struct. Mol. Biol. 18 (2011) 1218–1226.
[15] M. Landthaler, D. Gaidatzis, A. Rothballer, P.Y. Chen, S. Soll, L. Dinic, T. Ojo, M. Hafner, M. Zavolan, T. Tuschl, Molecular characterization of human Argonaute-containing ribonucleoprotein complexes and their bound target mRNAs, RNA 14 (2008) 2580–2596.
[16] L. Weinmann, J. Hock, T. Ivacevic, T. Ohrt, J. Mutze, P. Schwille, E. Kremmer, V. Benes, H. Urlaub, G. Meister, Importin 8 is a gene silencing factor that targets argonaute proteins to distinct mRNAs, Cell 136 (2009) 496–507.
[17] C.Y. Chu, T.M. Rana, Translation repression in human cells by microRNA-induced gene silencing requires RCK/p54, PLoS Biol. 4 (2006) e210.
[18] J.E. Braun, E. Huntzinger, M. Fauser, E. Izaurralde, GW182 proteins directly recruit cytoplasmic deadenylase complexes to miRNA targets, Mol. Cell 44 (2011) 120–133.
[19] H.H. Qi, P.P. Ongusaha, J. Myllyharju, D. Cheng, O. Pakkanen, Y. Shi, S.W. Lee, J. Peng, Y. Shi, Prolyl 4-hydroxylation regulates Argonaute 2 stability, Nature 455 (2008) 421–424.
[20] S. Li, L. Wang, B. Fu, M.A. Berman, A. Diallo, M.E. Dorf, TRIM65 regulates microRNA activity by ubiquitination of TNRC6, Proc. Natl. Acad. Sci. U. S. A. 111 (2014) 6970–6975.
[21] R. Kalantari, J.A. Hicks, L. Li, K.T. Gagnon, V. Sridhara, A. Lemoff, H. Mirzaei, D.R. Corey, Stable association of RNAi machinery is conserved between the cytoplasm and nucleus of human cells, RNA 22 (2016) 1085–1098.
[22] M. Kanehisa, Y. Sato, M. Kawashima, M. Furumichi, M. Tanabe, KEGG as a reference resource for gene and protein annotation, Nucleic Acids Res. 44 (2016) D457–D462.
[23] J.M. Coller, M. Tucher, U. Sheth, M.A. Valencia-Sanchez, R. Parker, The DEAD box helicase, Dhh1p, functions in mRNA decapping and interacts with both the decapping and deadenylase complexes, RNA 7 (2001) 1717–1727.

[24] N. Fischer, K. Weis, The DEAD box protein Dhh1 stimulates the decapping enzyme Dcp1, EMBO J. 21 (2002) 2788–3797.
[25] T. Miyasaka, M. Morita, K. Ito, T. Suzuki, H. Fukuda, S. Takeda, J. Inoue, K. Semba, T. Yamamoto, Interaction of antiproliferative protein Tob with the CCR4-NOT deadenylase complex, Cancer Sci. 99 (2008) 755–761.
[26] H. Tran, M. Schilling, C. Wirbelauer, D. Hess, Y. Nagamine, Facilitation of mRNA deadenylation and decay by the exosome-bound DExH protein RHAU, Mol. Cell 13 (2004) 101–111.
[27] M. Fenger-Gron, C. Fillman, B. Norrild, J. Lykke-Andersen, Multiple processing body factors and the ARE binding protein TTP activate RNA decapping, Mol. Cell 20 (2005) 905–915.
[28] S. West, N. Gromak, N.J. Proudfoot, Human 5′->3′ exonuclease Xrn2 promotes transcription termination at co-transcriptional cleavage sites, Nature 432 (2004) 522–525.
[29] A.E. Mayes, L. Verdone, P. Legrain, J.D. Beggs, Characterization of Sm-like proteins in yeast and their association with U6 snRNA, EMBO J. 18 (1999) 4321–4331.
[30] C.L. Denis, J. Chen, The CCR4-NOT complex plays diverse roles in mRNA metabolism, Prog. Nucleic Acid Res. Mol. Biol. 73 (2003) 221–250.
[31] Y.-T. Shirai, T. Suzuki, M. Morita, A. Takahashi, T. Yamamoto, Multifunctional roles of the mammalian CCR4-NOT complex in physiological phenomena, Front. Genet. 5 (2014) 286.
[32] C.G. Zwartjes, S. Jayne, D.L. van den Berg, H.T. Timmers, Repression of promoter activity by CNOT2, a subunit of the transcription regulatory Ccr4-not complex, J. Biol. Chem. 278 (2004) 10,848–10,854.
[33] G.S. Winkler, K.W. Mulder, V.J. Bardwell, E. Kalkhoven, H.M. Timmers, Human Ccr4-not complex is a ligand-dependent repressor of nuclear receptor-mediated transcription, EMBO J. 25 (2006) 3089–3099.
[34] J. Chen, J. Rappsilber, Y.C. Chiang, P. Russell, M. Mann, C.L. Denis, Purification and characterization of the 1.0 MDa CCR4-NOT complex identifies two novel components of the complex, J. Mol. Biol. 314 (2001) 683–694.
[35] T.K. Albert, H. Hanzawa, Y.I. Legtenberg, M.I.J. de Ruwe, F.A. van den Heuvel, M.A. Collart, R. Boelens, H.T. Timmers, Identification of a ubiquitin-protein ligase subunit within the CCR4-NOT transcription repressor complex, EMBO J. 21 (2002) 355–364.
[36] I. Behn-Ansmant, J. Rehwinkel, T. Doerks, A. Stark, P. Bork, E. Izaurralde, mRNA degradation by miRNAs and GW182 required both CCR4:NOT deadenylase and DCP1:DCP2 decapping complexes, Genes Dev. 20 (2006) 1885–1898.
[37] M.R. Fabian, M.K. Cieplak, F. Frank, M. Morita, J. Green, T. Srikumar, B. Nagar, T. Yamamoto, mRNA-mediated deadenylation is orchestrated by GW182 through two conserved motifs that interact with CCR4-NOT, Nat. Struct. Mol. Biol. 18 (2011) 1211–1217.
[38] C. Chen, K. Ito, A. Takahashi, G. Wang, T. Suzuki, T. Nakazawa, et al., Distinct expression patterns of the subunits of the CCR4-NOT deadenylase complex during neural development, Biochem. Biophys. Res. Commun. 411 (2011) 360–364.
[39] H. Mathys, J. Basquin, S. Ozgur, M. Czarnocki-Cieciura, F. Bonneau, A. Aartse, et al., Structural and biochemical insights to the role of the CCR4-NOT complex and DDX6 ATPase in microRNA repression, Mol. Cell 54 (2014) 751–765.
[40] P. Bawankar, B. Loh, L. Wohlbold, S. Schmidt, E. Izaurralde, NOT10 and C2orf29/NOT11 form a conserved module of the CCR4-NOT complex that docks onto the NOT1 N-terminal domain, RNA Biol. 10 (2013) 228–244.
[41] J. Basquin, V.V. Roudko, M. Rode, C. Basquin, B. Séraphin, E. Conti, Architecture of the nuclease module of the yeast Ccr4-not complex: the Not1-Caf1-Ccr4 interaction, Mol. Cell 48 (2012) 207–218.
[42] A.P. Petit, L. Wohlbold, P. Bawankar, E. Huntzinger, S. Schmidt, E. Izaurralde, et al., The structural basis for the interaction between the CAF1 nuclease and the NOT1 scaffold of the human CCR4-NOT deadenylase complex, Nucleic Acids Res. 40 (2012) 11,058–11,072.
[43] A. Boland, Y. Chen, T. Raisch, S. Jonas, O. Kuzuoğlu-Öztürk, L. Wohlbold, et al., Structure and assembly of the NOT module of the human CCR4-NOT complex, Nat. Struct. Mol. Biol. 20 (2013) 1289–1297.
[44] E. Wagner, S.L. Clement, J. Lykke-Andersen, An unconventional human Ccr4-Caf1 deadenylase complex in nuclear cajal bodies, Mol. Cell. Biol. 27 (2007) 1686–1695.
[45] G.E. Wise, L. Goldstein, Electron microscope localization of nuclear RNA's that shuttle between cytoplasm and nucleus and nuclear RNA's that do not, J. Cell Biol. 56 (1973) 129–138.
[46] G. Meister, Argonaute proteins: functional insights and emerging roles, Nat. Rev. Genet. 14 (2013) 447–459.
[47] S.I.S. Grewal, S. Jia, Heterochromatin revisited, Nat. Rev. Genet. 8 (2007) 35–46.
[48] K.V. Morris, S. Santoso, A.-M. Turner, C. Pastori, P.G. Hawkins, Bidirectional transcription directs both transcriptional gene activation and suppression in human cells, PLoS Genet. 4 (2008) e1000258.
[49] D.H. Kim, L.M. Villeneuve, K.V. Morris, J.J. Rossi, Argonaute-1 directs siRNA-mediated transcriptional gene silencing in human cells, Nat. Struct. Mol. Biol. 13 (2006) 793–797.
[50] Y. Chu, X. Yue, S.T. Younger, B.A. Janowski, D.R. Corey, Involvement of argonaute proteins in gene silencing and activation by RNAs complementary to a non-coding transcript at the progesterone receptor promoter, Nucleic Acids Res. 38 (2010) 7736–7748.
[51] V. Huang, J. Zheng, Z. Qi, J. Wang, R.F. Place, J. Yu, H. Li, L.-C. Li, Ago1 interacts with RNA polymerase II and binds to the promoters of actively transcribed genes in human cancer cells, PLoS Genet. 9 (2013) e1003821.
[52] M. Alló, V. Buggiano, J.P. Fededa, E. Petrillo, I. Schor, M. de la Mata, E. Agirre, M. Plass, E. Eyras, S.A. Elela, et al., Control of alternative splicing through siRNA-mediated transcriptional gene silencing, Nat. Struct. Mol. Biol. 16 (2009) 717–724.
[53] W. Wei, Z. Ba, M. Gao, Y. Wu, Y. Ma, S. Amiard, C.I. White, J.M. Rendtlew Danielsen, Y.-G. Yang, Y. Qi, A role for small RNAs in DNA double-strand break repair, Cell 149 (2012) 101–112.
[54] M. Gao, W. Wei, M.-M. Li, Y.-S. Wu, Z. Ba, K.-X. Jin, M.-M. Li, Y.-Q. Liao, S. Adhikari, Z. Chong, et al., Ago2 facilitates Rad51 recruitment and DNA double-strand break repair by homologous recombination, Cell Res. 24 (2014) 532–541.
[55] Y. Wei, L. Li, D. Wang, C.Y. Zhang, K. Zen, Importin 8 regulates the transport of mature microRNAs into the cell nucleus, J. Biol. Chem. 289 (2014) 10,270–10,275.
[56] A. Nishimura, K. Yamamoto, M. Oyama, H. Kozuka-Hata, H. Saito, K. Tatebayashi, Scaffold protein Ahk1, which associates with Hkr1, Sho1, Ste11, and Pbs2, inhibits cross talk signaling from the Hkr1 osmosensor to the Kss1 mitogen-activated protein kinase, Mol. Cell. Biol. 36 (2016) 1109–1123.
[57] D.W. Huang, B.T. Sherman, R.A. Lempicki, Systematic and integrative analysis of large gene lists using DAVID bioinformatics resources, Nat. Protoc. 4 (2009) 44–57.
[58] D.W. Huang, B.T. Sherman, R.A. Lempicki, Bioinformatics enrichment tools: paths toward the comprehensive functional analysis of large gene lists, Nucleic Acids Res. 37 (2009) 1–13.